The Astrophysical Journal, 965:22 (12pp), 2024 April 10 https://doi.org/10.3847/1538-4357/ad2f2c

Young Star Clusters Dominate the Production of Detached Black Hole–Star Binaries

Ugo Niccolò Di Carlo[1,2,3], Poojan Agrawal[2,3], Carl L. Rodriguez[2,3], and Katelyn Breivik[4]
[1] Scuola Internazionale Superiore di Studi Avanzati (SISSA), Via Bonomea 265, I-34136 Trieste, Italy; udicarlo@sissa.it
[2] Department of Physics and Astronomy, University of North Carolina at Chapel Hill, 120 E. Cameron Avenue, Chapel Hill, NC 27599, USA
[3] McWilliams Center for Cosmology, Department of Physics, Carnegie Mellon University, 5000 Forbes Avenue, Pittsburgh, PA 15213, USA
[4] Center for Computational Astrophysics, Flatiron Institute, 162 Fifth Avenue, New York, NY 10010, USA
Received 2023 June 26; revised 2024 February 15; accepted 2024 February 28; published 2024 April 2

Abstract

The recent discovery of two detached black hole–star (BH–star) binaries from Gaia's third data release has sparked interest in understanding the formation mechanisms of these systems. We investigate the formation of these systems by dynamical processes in young star clusters (SCs) and via isolated binary (IB) evolution, using a combination of direct *N*-body and population synthesis simulations. We find that dynamical formation in SCs is nearly 50 times more efficient per unit of star formation at producing BH–star binaries than IB evolution. We expand this analysis to the full Milky Way (MW) using a FIRE-2 hydrodynamical simulation of an MW-mass galaxy. Even assuming that only 10% of star formation goes into SCs, we find that approximately four out of every five BH–star systems are formed dynamically, and that the MW contains a total of $\sim 2 \times 10^5$ BH–star systems. Many of these dynamically formed systems have longer orbital periods, greater eccentricities, and greater black hole masses than their isolated counterparts. For binaries older than 100 Myr, we show that any detectable system with $e \gtrsim 0.5$ or $M_{\rm BH} \gtrsim 10\,M_\odot$ can *only* be formed through dynamical processes. Our MW model predicts between 64 and 215 such detections from the complete DR4 Gaia catalog, with the majority of systems being dynamically formed in massive and metal-rich SCs. Finally, we compare our populations to the recently discovered Gaia BH1 and Gaia BH2, and conclude that the dynamical scenario is the most favorable formation pathway for both systems.

Unified Astronomy Thesaurus concepts: Astrophysical black holes (98); Black holes (162); Stellar mass black holes (1611); Open star clusters (1160); Star clusters (1567); Young star clusters (1833); Gaia (2360); the Milky Way (1054); Binary stars (154)

1. Introduction

Current estimates anticipate that the Milky Way (MW) harbors a population of $\sim 10^7$–10^9 stellar black holes (BHs) and $\sim 10^4$ massive stars that are likely BH progenitors (Garmany et al. 1982; Reed 2003). While the exact binary fraction of stellar BHs is unknown, the high binary fraction of BH-progenitor stars (e.g., Sana et al. 2012) suggests that a substantial number of their BH descendants likely exist in binaries as well. Most of the current observational evidence for BH binary systems in the MW comes from X-ray binary systems, consisting of 20 dynamically confirmed BHs in X-ray binaries, with an additional ∼50 X-ray sources identified as strong candidates for containing BHs (McClintock et al. 2006; Remillard & McClintock 2006; Corral-Santana et al. 2016). However, population synthesis models indicate that the majority of BHs in binary systems within the MW are likely to be dormant BHs, with long orbital periods that preclude their involvement in X-ray binaries (Portegies Zwart et al. 1997; Corral-Santana et al. 2016; Breivik et al. 2017; Chawla et al. 2022), making them harder to detect. Over the past few years, it has become possible to identify dormant BHs through the motion of their luminous companions, with the first of these binaries being identified through the radial velocity of their luminous components in the globular cluster (GC) NGC 3201 (Giesers et al. 2018, 2019). More recently, proper motion data from ESO Gaia's Data Release 3 (DR3, Gaia Collaboration et al. 2022) has enabled the discovery of two dormant BHs in BH–star binary systems in the Galactic field (Chakrabarti et al. 2022; El-Badry et al. 2023a, 2023b; Tanikawa et al. 2023b). Combined with follow-up radial velocity measurements to fully characterize the orbit (El-Badry et al. 2023a, 2023b), these systems offer new insights into the formation, evolution, and characteristics of BHs in our Galaxy. The first system, Gaia BH1, consists of a Sun-like main-sequence (MS) star orbiting a black hole with mass $M_{\rm BH} = 9.62\,M_\odot$, eccentricity $e = 0.45$, and orbital period $P = 185.6$ days (El-Badry et al. 2023a). Gaia BH2 is a $\sim 1\,M_\odot$ red giant orbiting a black hole with mass $M_{\rm BH} = 8.9\,M_\odot$, eccentricity $e = 0.52$, and orbital period $P = 1277$ days (El-Badry et al. 2023b). According to El-Badry et al. (2023a, 2023b), the formation histories of both Gaia BH1 and Gaia BH2 are extremely difficult to explain by isolated binary (IB) evolution, due to the incompatibility between their orbital properties and the outcomes predicted for common envelope evolution. Star clusters (SCs), on the other hand, are highly favored environments for the formation of such systems; not only can dynamical interactions significantly alter the orbital properties of primordial binaries, allowing them to follow other evolutionary pathways, but BH–star binaries and their progenitors may also dynamically assemble through binary exchanges and/or multibody encounters. Despite this, the thin-disk-like Galactic orbits and near-solar metallicities of the Gaia BHs suggest that they most likely did not form dynamically in an old, metal-poor GC. Young/open SCs, on the other hand, are dynamical systems with Galactic orbits and metallicities perfectly compatible with those of Gaia BHs.

Additionally, they are the birthplace of the vast majority of massive stars, which are the progenitors of compact objects (e.g., Lada & Lada 2003; Portegies Zwart et al. 2010). Hence, the majority of BHs in the MW have probably spent the first part of their life in young/open SCs undergoing dynamical interactions.

In this paper, we investigate the dynamical formation of binary systems consisting of a star and a BH in young/open SCs in the MW and via IB evolution. We use a large set of 3×10^3 N-body simulations of young/open SCs (from Di Carlo et al. 2020b), along with population synthesis simulations of IB evolution. We describe the population of BH–star binaries in the MW, predicting the number and properties of the intrinsic population, and the expected detections in Gaia DR3 and in future Gaia data releases. Finally, we compare our systems with Gaia BH1 and Gaia BH2 to understand their possible formation pathway, and conclude that both systems (and especially BH2) are more compatible with a dynamical formation scenario. Throughout this paper, we use "star" to refer to every luminous stellar type except for white dwarfs and neutron stars (further discriminating between MS stars and giants when appropriate).

2. Methods

2.1. Population of Star Clusters

The star cluster simulations used in this paper were performed with the same code and methodology as described in Di Carlo et al. (2019, 2020b). Dynamics is treated by the direct summation N-body code NBODY6++GPU (Wang et al. 2015), coupled with the population synthesis code MOBSE (Mapelli et al. 2017; Giacobbo et al. 2018), an upgraded version of BSE (Hurley et al. 2002). MOBSE includes prescriptions for core-collapse supernovae (Fryer et al. 2012), winds of massive stars (Giacobbo & Mapelli 2018), electron-capture supernovae (Giacobbo & Mapelli 2019), natal kicks with fallback (Giacobbo & Mapelli 2020) and (pulsational) pair instability supernovae (Mapelli et al. 2020). Orbital evolution due to gravitational-wave emission is treated with the equations from Peters (1964).

In this work, we analyze 3×10^3 simulations of young/open SCs, which are extensively discussed in Di Carlo et al. (2020a, 2020b, 2021) and are referred to as "set A" in Di Carlo et al. (2020b). The initial distribution of stars in space is modeled with fractal initial conditions (Küpper et al. 2011; Ballone et al. 2020, 2021; Torniamenti et al. 2021) to mimic the asymmetry and clumpiness of star-forming regions (Goodwin & Whitworth 2004). The initial stellar mass $M_{\rm SC}$ of every SC ranges from $10^3\,M_\odot$ to $3 \times 10^4\,M_\odot$. Each cluster mass is drawn from a $dN/dM_{\rm SC} \propto M_{\rm SC}^{-2}$ distribution, i.e., the initial mass function (IMF) of young SCs in the MW described in Lada & Lada (2003). We calculate the initial half-mass radius $r_{\rm h}$ using the relationship from Marks & Kroupa (2012).

The SC initial conditions are generated using MCLUSTER (Küpper et al. 2011). We adopt the IMF from Kroupa (2001), with a minimum stellar mass of $0.1\,M_\odot$ and a maximum stellar mass of $150\,M_\odot$. The initial total binary fraction is $f_{\rm bin} = 0.4$. Mass ratios are drawn from a distribution $\mathcal{P}(q) \propto q^{-0.1}$ (where $q = m_2/m_1 \in [0.1,\ 1]$, Sana et al. 2012). All the stars with $m \geqslant 5\,M_\odot$ are in binary systems, while the stars with $m < 5\,M_\odot$ are paired stochastically until the initial binary fraction is reached. This is consistent with the multiplicity properties of O/B-type stars (Sana et al. 2012; Moe & Di Stefano 2017). Eccentricities and orbital periods are drawn from the distributions from Sana et al. (2012).

We set the efficiency of common envelope ejection to $\alpha = 5$. We adopt the rapid core-collapse supernovae model, described in Fryer et al. (2012). Natal kicks are randomly drawn from a Maxwellian velocity distribution. A one-dimensional rms velocity $\sigma = 15\,{\rm km\,s^{-1}}$ is adopted for both core-collapse supernovae and electron-capture supernovae. We have simulated SCs with three different metallicities: $Z = 0.02$, 0.002, and 0.0002. Each SC is simulated for 100 Myr in a static solar neighborhood-like tidal field (Wang et al. 2016). From each simulation, we extract all the binaries composed of a BH and a luminous companion that are still in the SC at the end of the simulations, as well as all the binaries of the same type that escape the SC.

2.2. Synthetic MW of Binaries and Clusters

Following Chawla et al. (2022), we seed both IBs and SCs following the star formation history of a cosmological zoom-in simulation of an MW-mass galaxy (specifically the `m12i` galaxy from the *Latte* simulations, Wetzel et al. 2016) from the Feedback In Realistic Environments (FIRE-2) suite of galaxies (Hopkins 2015; Hopkins et al. 2018). We extract from the publicly available data every star particle formed in the simulation (which each have a mass at formation of 7070 $M_\odot$), including the particle's metallicity and formation time. These are then binned into low ([Fe/H] < -1.5), intermediate ($-1.5 <$ [Fe/H] < -0.5), and high ($-0.5 <$ [Fe/H]) metallicity bins, designed to match the metallicities of the original `nbody6++gpu` cluster simulations. Each metallicity bin is then further divided into 100 equal intervals of cosmic time between 0 and 13.78 Gyr, providing us with the metallicity-dependent star formation rate of our MW-analog galaxy. Further details on the evolution of the star formation rate of the `m12i` galaxy as a function of metallicity can be found in Ma et al. (2017).

To convert this star formation per unit time into stars and clusters, we begin by assuming that all star formation occurs in clusters (Lada & Lada 2003). Since the lowest-mass clusters from Di Carlo et al. (2021) begin at 1000 $M_\odot$, we assume that all star formation clumps between 100 and 1000 $M_\odot$ may experience rapid dissolution into isolated stars and binaries due to processes such as infant mortality or the effects of the tidal field of the galaxy. While we acknowledge that there may be contributions from clusters in the 100–1000 $M_\odot$ range that we are currently ignoring,[5] the complications associated with accurately modeling infant mortality and gas expulsion make it significantly challenging to incorporate these effects into our current models. Meanwhile, clusters above 1000 $M_\odot$ are assumed to remain bound and undergo dynamical encounters. Along with our cluster IMF ($dN/dM_{\rm SC} \propto M_{\rm SC}^{-2}$), this suggests that 10% of star formation should occur in open clusters.

We seed our clusters in the `m12i` galaxy in the following way: for each bin of star formation, we draw randomly with replacement from the cluster sample, subtracting that cluster's mass from the total mass of star particles formed in that bin, until we have completely turned that 10% of the star formation into clusters. Each time we draw a cluster, we randomly pick an

[5] See Rastello et al. (2023) for an extensive analysis of BH–star binaries in SCs with masses smaller than 1000 $M_\odot$.

m12i star particle from the same time/metallicity bin, and assign that particle's exact formation time and present-day position in the m12i galaxy to the BH–star binaries produced by that cluster. Note that this procedure generates more clusters than are present in the original catalog, meaning that many of our dynamical sources are sampled repeatedly.

The remaining 90% of star formation is turned into massive binaries in a similar fashion: for each time/metallicity bin, the remaining star formation is converted directly into star particles, assuming the primary masses (that will become BHs) follow a $1/M^{2.3}$ IMF starting at 18 $M_\odot$ (Kroupa 2001) and up to 150 $M_\odot$, while the secondaries are drawn from a uniform distribution of mass ratio (Mazeh et al. 1992; Goldberg & Mazeh 1994) from 0.1 $M_\odot$ up to the primary masses. We apply an IMF correction to our synthesized binary population, to take into account that we only simulate the systems with at least one component that is a black hole progenitor. The binary orbital periods and the eccentricities are drawn from the same distributions as those assumed in Section 2.1. These systems are then evolved to the present day as described in the next section. For the m12i galaxy, this procedure yields approximately 9.4×10^7 binaries with at least one BH progenitor.

2.3. Evolving Binaries to the Present Day

For consistency with El-Badry et al. (2023a, 2023b), we evolve both IB and SC binaries to the present day using the binary population synthesis code COSMIC (Breivik et al. 2020). The binaries are evolved using the same stellar and binary evolution parameters and recipes as used in Di Carlo et al. (2020b), described in Section 2.1, to ensure that binary evolution is treated identically in both populations. IBs are evolved starting from the zero-age main sequence with absolute metallicities of 0.02, 0.002, and 0.0002 (to match the original cluster simulations), from the time when they were formed ($T_{\rm form}$) in the galaxy until the current age of the Universe (13.78 Gyr).

The evolution of SC binaries is restarted from the last recorded state of the binary in the *N*-body simulation—that is, either the time of binary ejection or the end of the cluster simulation at 100 Myr. Restarting the evolution of cluster binaries yields additional complications, because the binary evolution in COSMIC for systems having undergone mass loss or accretion depends on the current mass of the star, its effective initial mass, and the change in its effective age due to the mass loss/transfer (referred to as $M(t)$, M_0, and the stellar "epoch" in Hurley et al. 2000, respectively). M_0 and epoch are not part of the default nbody6++gpu output, but since we are primarily interested in BHs and MS stars, this did not present a major difficulty: in COSMIC, M_0 is equal to M_t for both BHs and MS stars, while the epoch is only relevant for the calculations of evolution of MS stars. We assume epoch = 0 Myr for MS stars when restarting their evolution. As a test, we ran the entire population with epoch values of 0 and 100 Myr (the minimum and maximum values it could have given the SC integration time) and found the difference in the population-level statistics to be negligible (only 1% of systems show a relative difference greater than ∼1% in their final masses and orbital periods between epoch = 0 Myr and epoch = 100 Myr). While restarting post-MS stars in COSMIC is substantially more complicated, none of the luminous companion stars evolved beyond the MS before the end of the SC simulations (as opposed to evolving onto the giant branch later in the galactic field). In our analysis, we distinguish between BH–MS binaries and BH–giant binaries. We follow the criterion from Drout et al. (2012) and classify post-MS stars with $T_{\rm eff} \leqslant 4800$ K as giants. This includes stars with BSE stellar types associated with red giants, core helium-burning stars, and asymptotic giant branch stars (types 3, 4, and 5).

For our analysis, we only select systems with an age $t_{\rm age} \geqslant 100$ Myr. This choice is justified for three reasons: first, our SCs are evolved for 100 Myr, and therefore we are unable to accurately track systems within SCs that formed in the past 100 Myr. Second, the star formation history of the FIRE-2 simulations can be larger than that observed in MW-mass galaxies at late times by a factor of a few (Section 4.5 of Hafen et al. 2022). This is true in particular for the m12i galaxy we consider, whose $z = 0$ star formation rate (6 $M_\odot\,{\rm yr}^{-1}$, Wetzel et al. 2016) is $\gtrsim$3–4 times the best observational estimate of star formation in the MW (1.65 ± 0.19 $M_\odot\,{\rm yr}^{-1}$, Licquia & Newman 2015). Finally, one of the main focuses of this paper is to understand the formation channels of Gaia BH1 and Gaia BH2, which are both older than ∼1 Gyr (and likely significantly older, especially in the case of Gaia BH2, El-Badry et al. 2023a, Section 3.8). We briefly discuss the implications of this cutoff (and what our results would look like including such systems) in Section 5.3.

2.4. Gaia Detectability

Following Chawla et al. (2022), we further determine whether Gaia can astrometrically resolve each orbit based on the motion of the luminous companion using optimistic and pessimistic criteria. As a starting point, based on the distance and position of each source on the sky, we calculate the photometric signature of each luminous component in the binary by converting from bolometric luminosities to Gaia apparent G using isochrones (Morton 2015). We then apply dust extinction and reddening along the line of sight to each system using a combined three-dimensional dust map based on Drimmel et al. (2003), Marshall et al. (2016), and Green et al. (2019) as implemented in mwdust (Bovy et al. 2016). We assume that systems are photometrically detectable if the luminous companion's reddened and extincted apparent magnitude is brighter than $G = 20$. Finally, we assign a random orientation to each binary and project the orbit of the luminous companion onto the sky using the Thiele–Innes elements. In the optimistic case, we assume that Gaia can resolve any orbit for which the star's projected motion is at least as large as Gaia's single pointing precision, σ_G, when it is projected on the plane of the sky and where σ_G is assumed to follow Lindegren et al. (2018). In the pessimistic case, we require the projected star's orbit to be at least three times as large as σ_G.

We also consider the cut in the parallax signal-to-noise ratio (S/N), ω/σ_ω, which was applied in Gaia DR3. This cut was applied as a function of orbital period as shown in Figure 1 to address spurious measurements of orbital period that were due to the Gaia scanning pattern. For a detailed discussion of these effects, see Holl et al. (2023). For each binary that is deemed detectable in the optimistic or pessimistic cases described above, we calculate the parallax and parallax error based on the position and extinction-corrected brightness of each luminous companion. The results are shown for the SC BH–star binaries in red and IB binaries in blue. Dynamically formed BH–star

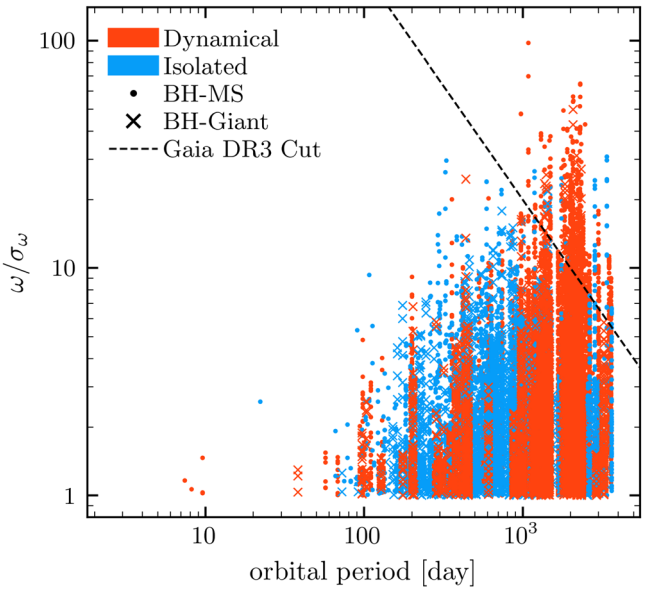

Figure 1. The orbital period vs. parallax S/N, ω/σ_ω, is shown for BH–star binaries formed in clusters (red) and in isolated binaries (blue) from all of our 100 MW-like simulation realizations. Dots show BH–MS binaries and crosses show BH–giant binaries. The dashed black line shows the parallax S/N cut placed as a function of orbital period for Gaia DR3 such that only binaries above the line are included in the data set.

binaries are preferentially located above the S/N cut while IB BH–star binaries that lie above the cut are mostly due to random-chance placements that are unrealistically close to Earth.

To increase our statistical sample of "detected" systems, we consider different positions for Earth in the `m12i` simulation and combine the results. We use 100 different equally spaced starting positions along a ring in the disk with radius 8.5 kpc. For what follows, the results for our synthetic Gaia population are divided by 100 when quoting the number of detectable binaries and all other relevant quantities.

3. Results

3.1. Intrinsic Population

We first explore the intrinsic population of BH–star binary systems in the galaxy; that is, the full population before considering our Gaia detectability criterion. In all our BH–star systems, the luminous member is either an MS or giant star. The exact numbers of systems per formation channel and stellar type are reported in Table 1. Based on the `m12i` simulation, we predict that the MW hosts a total of $\sim 2 \times 10^5$ BH–star systems from the IB and the young/open SC channels, with ∼86% of the systems formed dynamically and ∼14% formed in isolation. This means that, according to our models, SCs produce nearly six times more systems than IBs. However, we must emphasize that we have assumed that only 10% of the star formation occurs in young SCs. If we take this into account, it is obvious that SCs are *dramatically* more efficient than IBs at producing BH–star systems, with SCs producing ∼50 times as many systems overall, per unit mass, as IB evolution. This is driven largely by the production of BH–MS star systems: SCs produce 10 times more BH–giant binaries than IBs.

Figure 2 shows the distribution of the orbital parameters of the systems in the intrinsic population. SCs are much more efficient at producing systems with long orbital periods for both

Table 1
Formation Efficiency, Total Number of BH–Star Binary Systems (Intrinsic Population), Number of Expected Gaia DR3 Detections, and Number of Pessimistic–Optimistic Expected Gaia Detections Including Future Data Releases

Channel	All	BH–MS	BH–Giant
	Formation Efficiency ($M_\odot^{-1}$)		
Isolated	3.32×10^{-7}	3.19×10^{-7}	1.34×10^{-8}
Dynamical	1.81×10^{-5}	1.80×10^{-5}	1.25×10^{-7}
Dynamical Esc.	3.31×10^{-6}	3.29×10^{-6}	2.29×10^{-8}
Total	2.11×10^{-6}	2.09×10^{-6}	2.46×10^{-8}
	Intrinsic Population		
Isolated	25,719	24,678	1041
Dynamical	155,724	154,650	1074
Dynamical esc.	25,456	28,259	197
Total	181,443	179,328	2115
	Gaia DR3 Detections		
Isolated	0.4	0.4	0.0
Dynamical	6.7	5.6	1.1
Dynamical esc.	1.2	1.1	0.1
Total	7.1	6.0	1.1
	Gaia Detections (Including Future Data Releases)		
Isolated	12–44	7–24	5–20
Dynamical	52–171	40–126	12–45
Dynamical esc.	8–24	6–18	2–6
Total	64–215	47–150	17–65

Note. The formation efficiency is the number of systems in the intrinsic population produced per unit simulated stellar mass. Column (1): formation channel of the binary; column (2): value for all BH–star binaries; column (3): value for BH–main-sequence binaries only; column (4): value for BH–giant binaries only. Decimal values come from our average over 100 different observations (see Section 2.4). For Gaia DR3 detections, our optimistic and pessimistic values are identical. The Dynamical esc. channel only includes binaries that escape from the host SC before the end of the *N*-body simulations. The total refers to the isolated and the dynamical channels put together.

BH–MS and BH–giant binaries. IB systems have eccentricities up to ∼0.84, while the most eccentric dynamical system has an eccentricity of ∼0.99. IBs produce fewer systems with more massive stars: the maximum value of M_* for IBs is $\sim 5\,M_\odot$, while it is $\sim 7\,M_\odot$ for SCs (though this does depend on the 100 Myr cutoff we have employed, as described in Section 5.3). The maximum BH mass is $\sim 50\,M_\odot$ for IBs and $\sim 67\,M_\odot$ for the SC channel. The SC channel is thus able to form systems with eccentricities and masses hardly accessible with IB evolution. We also highlight that ∼85% of the BH–star binaries formed in SCs are retained by their host SC at the end of the simulations. Despite the relatively low initial mass of the SCs considered in this study, most of them have not undergone complete disruption by the end of the simulations and could possibly survive longer (see, e.g., Torniamenti et al. 2022). While it is possible that some of the retained binaries may eventually disrupt due to dynamical encounters, it is also highly likely that new BH–star binaries will form as a result of ongoing dynamical interactions. In Table 1, we additionally show results from the subset comprising solely the binaries that have escaped from their host SC. These results serve as conservative lower limits for our findings.

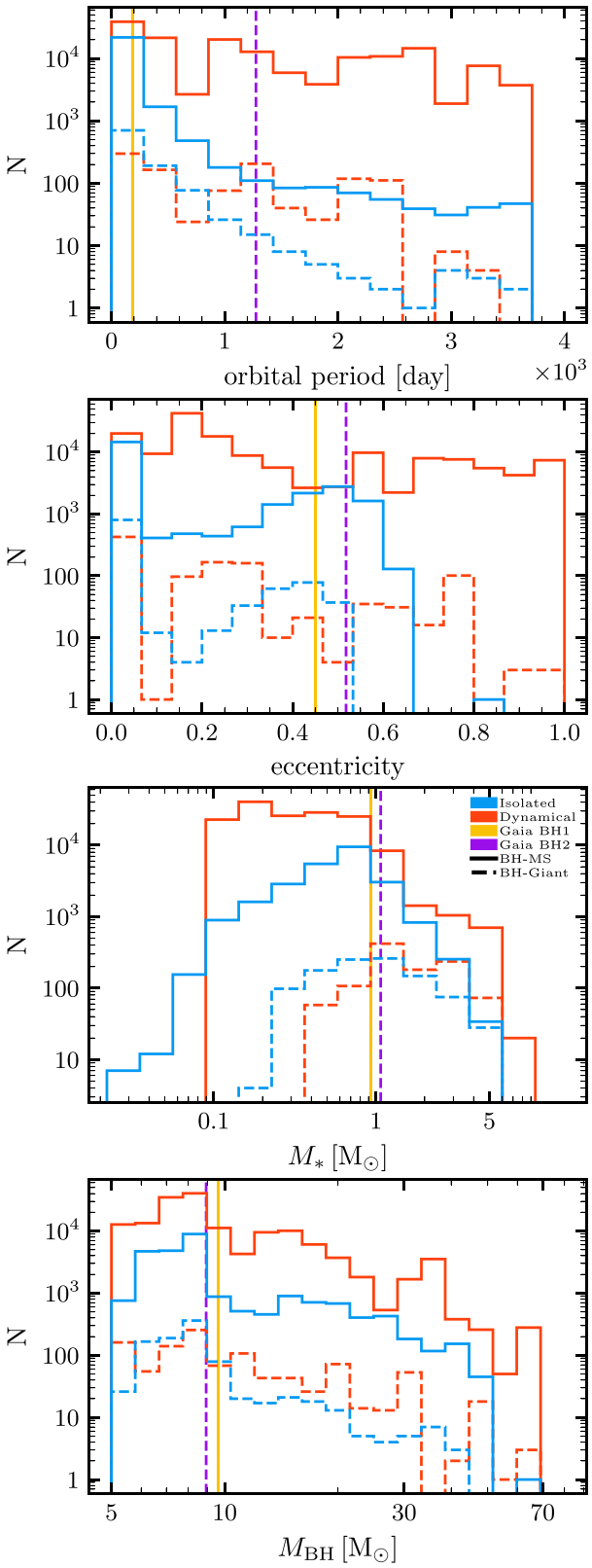

Figure 2. Orbital parameters of systems in the intrinsic population. From top to bottom we show the distributions of binary orbital periods, eccentricities, stellar masses M_*, and BH masses $M_{\rm BH}$, with SC binaries shown by red lines and IB shown by blue lines. Solid lines represent BH–MS binaries, while dashed lines show BH–giant binaries. The yellow and purple vertical lines represent the values of Gaia BH1 and Gaia BH2 respectively.

3.2. Population Detectable by Gaia

The Gaia mission provides a unique opportunity to detect a subset of the intrinsic population of BH–star binary systems in the Milky Way. Table 1 presents the number of systems in our data set according to their detectability by Gaia. The table displays two subsets: the first contains the number of systems detectable by Gaia DR3 in our model, while the second includes systems detectable by both Gaia DR3 and future Gaia data releases. It is evident how SCs are significantly more efficient at producing detectable binaries. In particular, we see that all the seven expected Gaia DR3 detections are expected to come from the dynamical formation channel. If we also consider detections with future Gaia data releases, we predict that Gaia will detect between 12 and 44 binaries from IBs, and between 52 and 171 binaries from the dynamical channel, i.e., a factor of ∼4 more dynamical systems. In general, our models produce more detectable BH–MS binaries than BH–giant binaries.

Figure 3 shows the distributions and correlations of the orbital parameters for the detectable population. It is evident that only SCs are able to produce detectable systems with large eccentricities and with large BH masses. In particular, the detection of a system with $e \gtrsim 0.5$ or with $M_{\rm BH} \gtrsim 10\,M_\odot$ would be a smoking gun of dynamical formation, as IBs are unable to form detectable systems with these characteristics in our models. The SC channel is more efficient at producing detectable binaries with long orbital periods as well. However, we reiterate that these results are for systems older than 100 Myr; we explore the implications of this cutoff in Section 5.3.

3.3. Dynamical Formation and Star Cluster Properties

The results from our analysis of the intrinsic and detectable populations strongly suggest that the majority of these systems are formed dynamically in SCs. Given that, it is informative to understand how many detectable systems produced by SC evolution come from primordial binaries (i.e., binaries present in the SC since the beginning of the simulation that may have been altered through dynamical processes) or from binaries that were assembled later dynamically. We find that approximately 94% of detections stem from these dynamically assembled binaries, while the remaining 6% arise from primordial binaries; ∼20% of the dynamically assembled binaries initially assemble as a star–star system (which later evolves to a BH–star system), while the remaining ∼80% form dynamically from a BH and a star, via exchanges and three-body binary formation.

We can also ask which SCs produce the majority of the BH–star binaries. In Figure 4, we show the number of BH–star binaries produced by SCs of a given mass. Even though the cluster catalog is sampled following a $\propto M_{\rm SC}^{-2}$ cluster mass function (containing many more low-mass clusters), the intrinsic population exhibits a relatively uniform distribution across SC masses, while the detectable population predominantly arises from SCs with $M_{\rm SC} \gtrsim 3\times10^3\,M_\odot$. For insights into the formation of BH–MS binaries in SCs with lower masses ($M_{\rm SC} = 300$–$1000\,M_\odot$), Rastello et al. (2023) show a comprehensive analysis that compares results from low- and high-mass SCs.

The overwhelming majority of observable binary systems originate from SCs with high metallicity ($Z = 0.02$), with

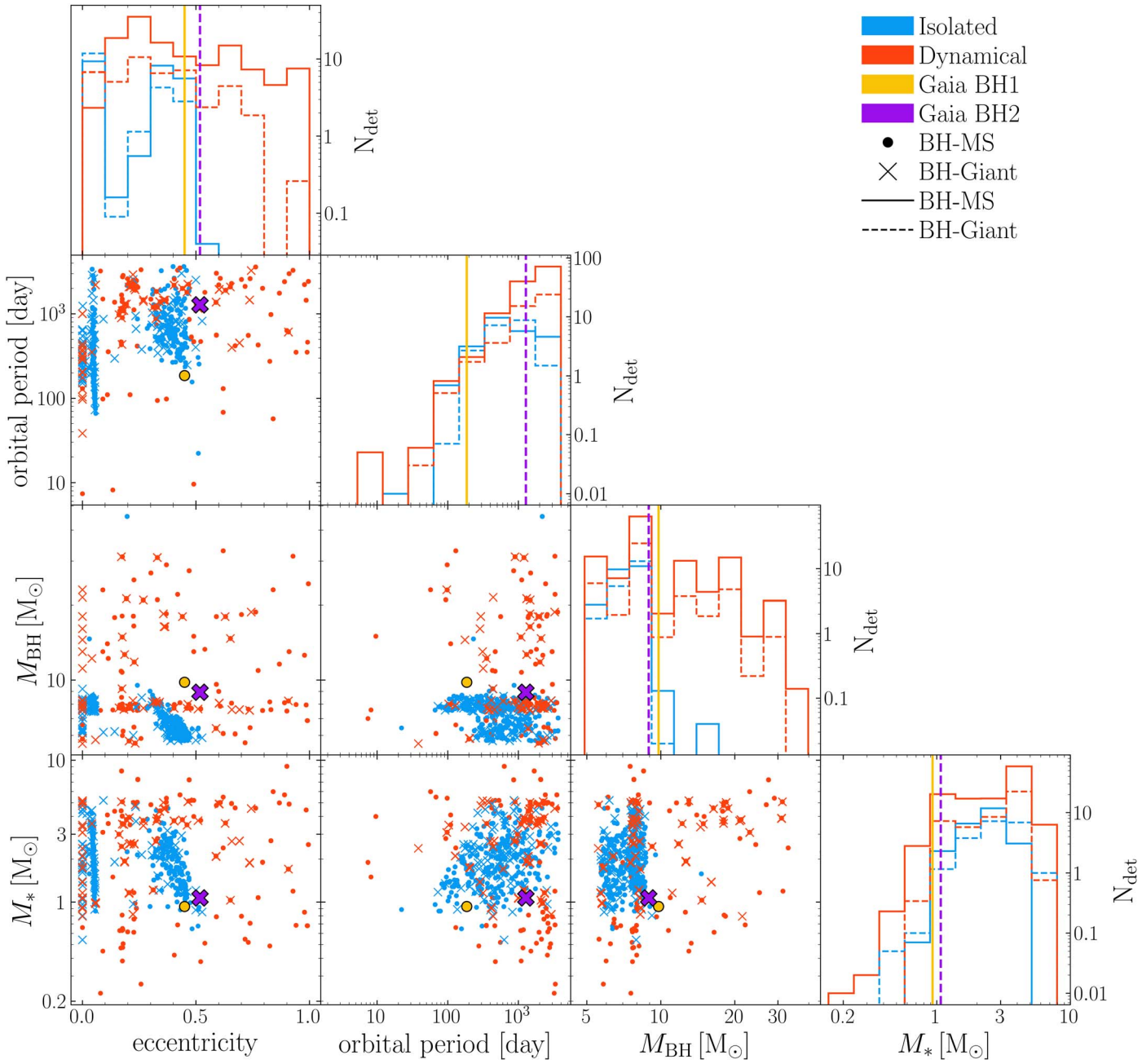

Figure 3. Correlations and distributions of orbital period, eccentricity, mass of the star, and mass of the BH of detectable systems. Dynamical systems are shown in red, while isolated systems are shown in blue. Gaia BH1 is shown in yellow, while Gaia BH2 is shown in violet. BH–MS systems are represented by filled circles in the scatter panels and by solid lines in the histogram panels. BH–giant systems are represented by crosses in the scatter panels and by dashed lines in the histogram panels. Scatter plots show systems from all the 100 observers around the Galaxy (see Section 2.4), while histograms show the number of detections $N_{\rm det} = N/100$.

∼99.84% of them forming in such clusters. This is because of the metallicity-dependent star formation history of the MW. Massive metal-rich SCs are thus very efficient at producing detectable binaries, and we expect the majority of BH–star systems in the MW and current/future Gaia detections to have formed in such environments. In a recent study, Tanikawa et al. (2024) estimated that the MW hosts around 1.6×10^4 Gaia BH-like star systems by simulating SCs with $M_{\rm SC} = 1000\,M_\odot$. Using the same criteria, our analysis suggests a larger number of $\sim 4 \times 10^4$ BH–star systems, highlighting the crucial role of more massive SCs in comprehending the formation and evolution of these systems.

4. Forming Gaia BH1 and Gaia BH2

In order to understand how the BH–star binary systems detected by Gaia might have formed, we compare their properties to those of our simulated populations. For both the IB and the SC channels, we find the most similar system to each of Gaia BH1 and Gaia BH2 in the detectable population, and describe their formation history. The identification of the most similar system entails assessing the fractional differences in key parameters, namely the orbital period, primary mass, and secondary mass, between the simulated binaries and the Gaia BHs. The fractional difference is defined as $|x - x_{\rm GAIA}|/x_{\rm GAIA}$, where x is the parameter of the object in the simulated population and $x_{\rm GAIA}$ is the corresponding parameter of the

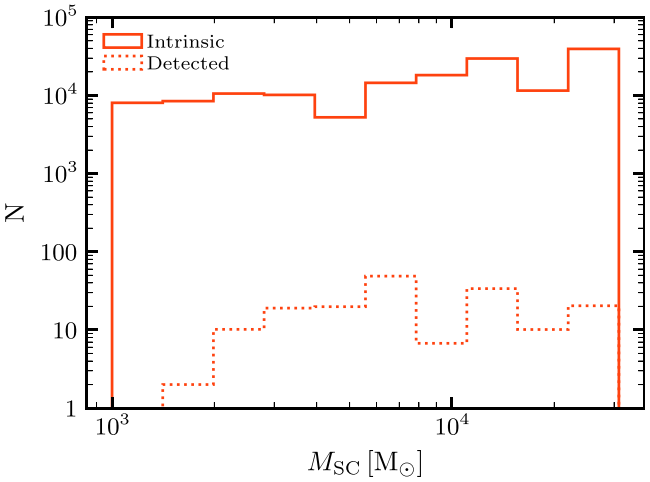

Figure 4. Distributions of the initial SC masses M_{SC} that produce BH–star binaries. The intrinsic population is shown by the solid red line, while the detectable population is shown by the dotted red line. The initial masses of the simulated SCs are drawn from a $dN/dM_{SC} \propto M_{SC}^{-2}$ distribution (Lada & Lada 2003), meaning that we simulated more low-mass SCs and fewer high-mass SCs.

Gaia BH. The system that exhibits the smallest maximum fractional difference across these parameters (i.e., the one that deviates the least across all the parameters considered) is regarded as the most similar to the Gaia BH. Due to the relatively limited statistical data available for the SC channel, we make the assumption that eccentricities are subject to randomization through dynamical encounters in SCs, where the eccentricity distribution is expected to follow a thermal profile. Thus, we exclude the eccentricity in the evaluation of the most similar systems. The formation histories of these systems are summarized in Figure 5.

4.1. Gaia BH1

The parameters of the most similar IB system to Gaia BH1 fall within approximately 25% of those of Gaia BH1. The system has an orbital period $P \sim 232$ days, $M_{BH} \simeq 8.4\ M_\odot$, and $M_* \simeq 1.05\ M_\odot$. The initial conditions of the system are $P \simeq 3486$ days, $M_1 \simeq 55.1\ M_\odot$, $M_2 \simeq 1.04\ M_\odot$, and a metallicity of $Z = 0.02$. The system undergoes a common envelope episode that significantly shrinks its orbit, and then turns into a BH–MS binary after 4.8 Myr. The binary then evolves unperturbed to the present day. The system has an age of ∼1.5 Gyr.

The closest system from the SC channel has parameters within ∼32% of Gaia BH1. The system has an orbital period $P \sim 130$ days, $M_{BH} \simeq 6.6\ M_\odot$, and $M_* \simeq 0.6\ M_\odot$. The system assembles dynamically inside an SC with metallicity $Z = 0.02$ and initial mass $M_{SC} = 3204\ M_\odot$. The binary forms ∼5 Myr after the beginning of the simulation. The primary turns into a giant, triggering a common envelope episode that shrinks the orbit. Afterwards, the envelope is ejected, and the primary turns into a BH. About 10 Myr after its formation, the system is dynamically ejected from the SC. The age of this system is ∼3 Gyr.

Both the IB and SC models struggle to reproduce a system that very closely resembles Gaia BH1. Rastello et al. (2023) suggest that the formation of Gaia BH1 might be explained by less massive SCs, with masses ranging from 300 $M_\odot$ to 1000 $M_\odot$. These lower-mass SCs could provide a favorable environment for the formation of a system with properties similar to Gaia BH1. Based on our analysis of the age distribution and of our detection rates for BH–MS systems in Gaia DR3, we draw the conclusion that the dynamical formation channel is the most favorable for Gaia BH1, as we explain more clearly in Section 5.2.

4.2. Gaia BH2

The closest IB system to Gaia BH2 is a BH–giant binary with $P \sim 1044$ days, $M_{BH} \simeq 8.0\ M_\odot$, and $M_* \simeq 1.3\ M_\odot$. The values lie within ∼19% of the parameters of Gaia BH2. The initial conditions of the system are $P \simeq 3967$ days, $M_1 \simeq 45.8\ M_\odot$, and $M_2 \simeq 1.36\ M_\odot$. The system has a metallicity of $Z = 0.02$, and undergoes a common envelope episode throughout its evolution. The system has an age of ∼4.1 Gyr, which is not compatible with the age of Gaia BH2.

The best candidate from the SC channel has parameters within 13% of the Gaia BH2 parameters. The system has an orbital period $P \sim 1197$ days, $M_{BH} \simeq 8.1\ M_\odot$, and $M_* \simeq 1.2\ M_\odot$. The binary is dynamically assembled in an SC with metallicity $Z = 0.02$, initial mass $M_{SC} = 14284\ M_\odot$, and an age of ∼6 Gyr. The system forms as a BH–MS binary ∼39 Myr after the beginning of the simulation, and it later evolves to a BH–giant. The system is retained by its host SC at the end of the simulation.

Both channels produce systems that exhibit close parameter matches to Gaia BH2. Among these, the dynamical scenario yields the closest resemblance. If we also take into account that Gaia BH2 is estimated to be older than 5 Gyr, and that our Gaia DR3 detections for BH–giant systems come entirely from SCs, we conclude that Gaia BH2 has likely formed via the dynamical formation channel. We provide a more extensive analysis of this in Section 5.2.

5. Discussion

5.1. Dynamical versus Isolated

We see from Table 1 that the dynamical channel produces ∼6 times more BH–star systems than the isolated channel. Since we consider that only 10% of the total star formation occurs in SCs, we find that the number of systems produced per unit stellar mass by SCs is ∼50 times larger than the number of systems produced by isolated binary evolution. This discrepancy can be attributed to several mechanisms. Stellar dynamics in SCs significantly affects the formation and evolution of binaries. Multibody encounters can dynamically assemble BH–star or star–star binaries that can later evolve into BH–star binaries, resulting in combinations of orbital parameters that are inaccessible in IB evolution. Furthermore, three-body encounters between a binary and a single object can modify the eccentricity and orbital period of binaries, triggering or preventing mass transfer episodes (e.g., Roche-lobe overflow and common envelope evolution) that may or may not occur if the binary were to evolve in isolation. Common envelope episodes significantly reduce the orbital period of binaries. From Figures 2 and 3, we see how the dynamical channel is extremely more efficient at producing binaries with longer orbital periods. Indeed, we find that every simulated IB system that becomes a BH–star binary undergoes at least one common envelope episode throughout its evolution. This can be easily avoided in SCs; as we said in Section 3.3, the majority of detectable SC binaries dynamically assemble as BH–star

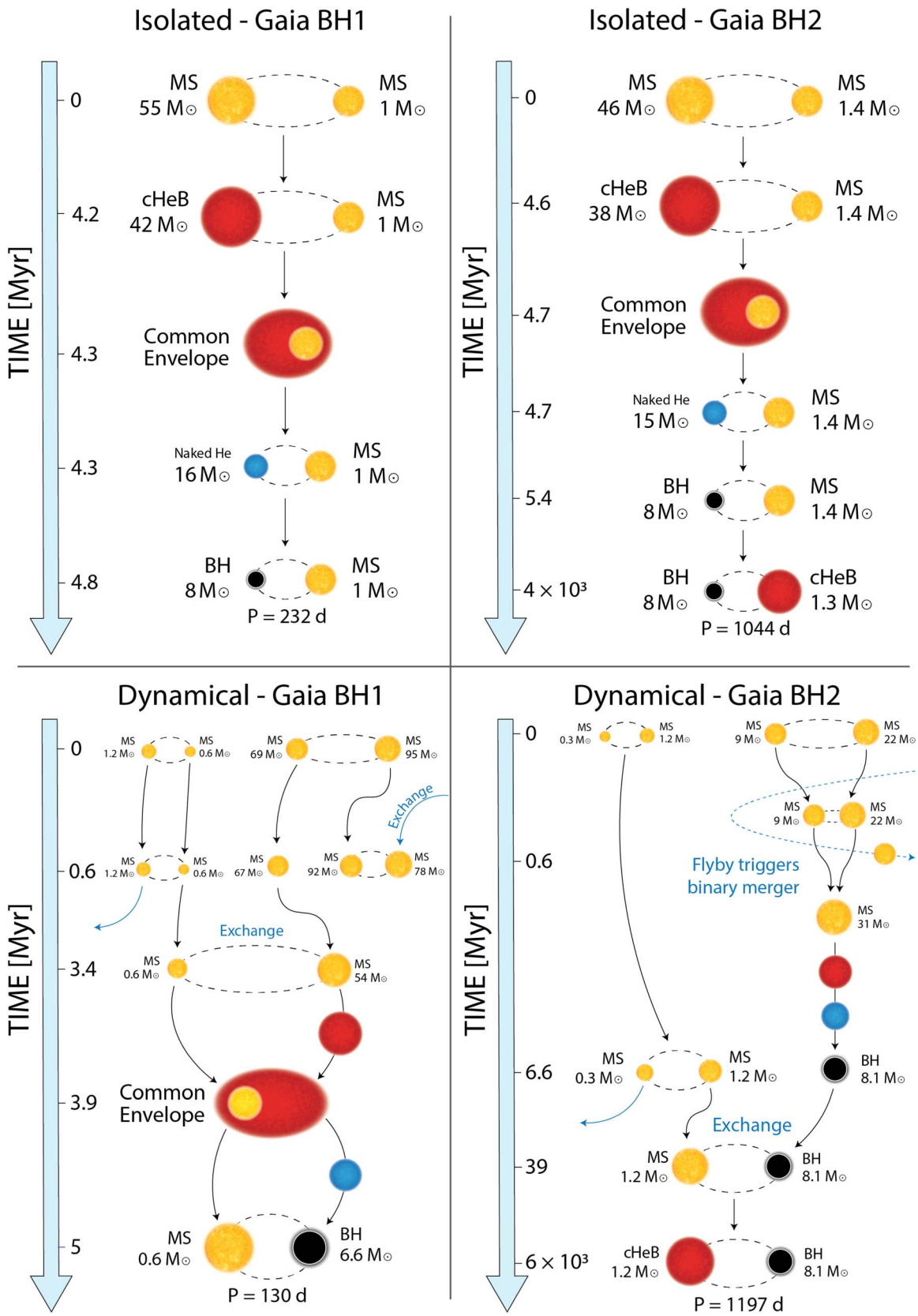

Figure 5. Formation history of the most similar systems to Gaia BH1 (left panels) and Gaia BH2 (right panels) in our simulations. Top panels show systems from the isolated binary evolution channel; bottom panels show systems from the star clusters channel. Main-sequence stars (with label MS) are represented as yellow stars; core helium-burning stars (label cHeB) are visualized as red stars; naked helium stars (label Naked He) are represented as blue stars; black holes (label BH) are shown as black circles. The mass of each object is shown next to it. The orbital period in days of the final binaries is shown underneath. The time axis and the size of the objects and orbits are not to scale. Even though Gaia BH-like systems can be formed by both the formation channels, our results on rates and ages presented in Section 5.2 strongly suggest that the dynamical scenario is the primary formation pathway for the Gaia BHs.

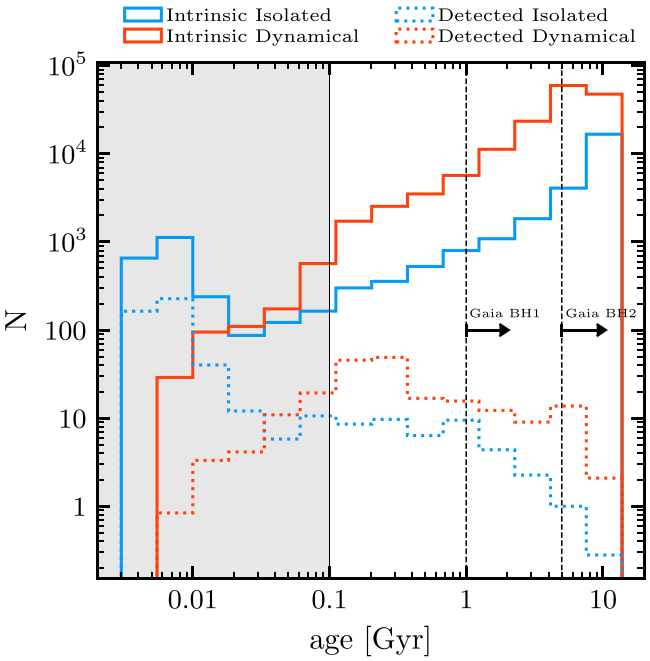

Figure 6. Distributions of the ages of systems in our data sets. The intrinsic population is shown by solid lines, while Gaia-detectable systems are shown by dotted lines. Dynamical systems are shown in red, while isolated systems are shown in blue. The two dashed vertical lines show the lower limits of the age of Gaia BH1 and Gaia BH2. The gray shaded area on the left represents the systems not taken into account due to the age cutoff described in Section 2.3.

binaries already, which means that they do not undergo a common envelope episode.[6] The dynamical channel is thus not only more efficient, but can also leave unique fingerprints on the properties of the binaries.

5.2. Formation Channels of Gaia BHs

Our models provide several hints on how the dynamical scenario is a more favorable formation pathway for Gaia BH1 and Gaia BH2. According to our results in Table 1, all the expected Gaia DR3 detections come from SCs, suggesting that Gaia BHs have more likely formed dynamically. In order to form systems like Gaia BH1 or Gaia BH2 through IB evolution, El-Badry et al. (2023a, 2023b) highlight the necessity of assuming an exceedingly large and potentially unrealistic value for the common envelope efficiency ($\alpha \approx 12.8$ for Gaia BH1). Lower values of α would have led to the merger of the binary components, preventing the formation of Gaia BHs through this channel. As discussed in Section 5.1, dynamics offers an alternative pathway for the formation of BH–star systems that completely bypasses the common envelope phase.

The age distribution of the detected systems is shown in Figure 6. The efficiency of the two channels is comparable below 0.1 Gyr, but the dynamical channel is much more efficient at forming detectable systems with older ages. Gaia BH1 has an age $\gtrsim$1 Gyr, while Gaia BH2 has an age $\gtrsim$5 Gyr,

[6] The only way for such binaries to undergo a common envelope episode and still be classified as BH–star binaries is if the following sequence of events occurs: (i) the star becomes a giant; (ii) its expansion triggers a common envelope; (iii) the envelope is ejected by the BH companion, leaving behind a BH and a naked He star. We do not find any BH–naked He star binary in our populations.

Table 2
Same as Table 1, but without the 100 Myr Formation Time Cutoff

Channel	All	BH–MS	BH–Giant
Formation Efficiency ($M_\odot^{-1}$)			
Isolated	3.63×10^{-7}	3.49×10^{-7}	1.39×10^{-8}
Dynamical	1.84×10^{-5}	1.83×10^{-5}	1.30×10^{-7}
Dynamical esc.	3.40×10^{-6}	3.37×10^{-6}	2.34×10^{-8}
Total	2.15×10^{-6}	2.12×10^{-6}	2.50×10^{-8}
Intrinsic Population			
Isolated	28,081	27,005	1076
Dynamical	156,478	155,400	1078
Dynamical esc.	29,210	29,009	201
Total	184,559	182,405	2154
Gaia DR3 Detections			
Isolated	103	101	2
Dynamical	10	9	1
Dynamical esc.	4	4	0
Total	113	110	3
Gaia Detections (Including Future Data Releases)			
Isolated	301–502	290–473	11–29
Dynamical	63–202	51–156	12–46
Dynamical esc.	19–55	17–47	2–8
Total	364–704	341–629	23–75

indicating that both Gaia BHs, particularly Gaia BH2, have likely formed dynamically, according to our models.

Rastello et al. (2023) show that both lower-mass (300–1000 $M_\odot$) and higher-mass (1000–30,000 $M_\odot$) young SCs are efficient in forming Gaia BH1–like systems. Gaia BHs may also have formed via other channels not taken into account in this study, such as formation in isolated hierarchical triples or hierarchical triples formed in SCs (see, e.g., Trani et al. 2022). Another plausible channel could be the dynamical formation in a globular cluster (GC); while the Galactic orbit of both Gaia BHs is not aligned with any GC in the MW (El-Badry et al. 2023a, 2023b), these systems might have dynamically formed in GCs that have already completely disrupted.

5.3. BH–Star Ages and the 100 Myr Age Cutoff

Throughout this paper, we have argued that SCs dominate the production of old BH–star systems in the MW. We show this explicitly in Figure 6, which displays the distribution of ages of the systems and reveals that the dynamical formation channel appears to be more efficient at producing older systems, particularly those older than 1 Gyr.

Of course, it is also obvious in Figure 6 that our 100 Myr cutoff has removed a large number of young systems, particularly from the IB channel, that contribute significantly to the detectable population. For comparison, we present the results obtained without applying the 100 Myr age cutoff (which was justified in Section 2.3), starting with Table 2, which reports the number of systems in the intrinsic and detectable populations. Although there is an increase in the number of systems in the isolated intrinsic population, the dynamical channel remains dominant, constituting approximately 85% of the total intrinsic population.

However, we observe a significant increase in the number of isolated detectable systems. The expected number of IB detections by Gaia DR3 increases from 0 to 103, while the total number of IB Gaia detections increases from 12–44 to 301–502. Conversely, the number of detectable systems from the dynamical channel barely increases. This disparity can be attributed to the fact that systems in the isolated population are predominantly very young (see Figure 6) and preferentially host bright massive stars that are significantly easier to detect. This trend is evident from Figures 7 and 8, which illustrate the significant impact of the cutoff on the M_* distribution. The difference comes almost entirely from a huge population of young massive O stars. The IB detectable systems younger than 20 Myr have an average BH mass of 8 $M_\odot$ and an average star mass of 41 $M_\odot$, and constitute ∼86% of the total number of detectable systems in the whole IB catalog without the 100 Myr age cutoff. We emphasize that our predictions for the formation channels of both Gaia BH1 and Gaia BH2 should remain unaffected by this cutoff, as they both are older than 1 Gyr.

6. Conclusions

The MW is very likely populated by a large number of stellar BHs, many of which probably reside in binary systems. The recent discovery of two BH–star binaries in Gaia DR3 has sparked new interest in understanding the formation channels and population characteristics of such systems. In this paper, we have investigated the formation of BH–star binaries in young SCs and via IB evolution.

According to our simulations, the MW harbors a total of $\sim 2 \times 10^5$ BH–star systems, of which ∼86% formed dynamically and ∼14% formed in isolation. We find that dynamical formation in SCs is nearly 50 times more efficient per unit stellar mass at producing BH–star binaries than isolated binary evolution. Dynamical systems tend to have longer orbital periods and greater eccentricities than isolated ones. We expect that a total of seven BH–star systems are present in the Gaia DR3 data, all of which come from the dynamical channel. We also predict between 64 and 215 detections from the whole Gaia mission, ∼80% of which come from SCs. Overall, dynamics enhances dramatically the number of BH–star binaries, in both the intrinsic and the detectable populations.

We compare our detectable populations with Gaia BHs, and we conclude that our models support the dynamical scenario as the primary formation pathway for Gaia BH1 and Gaia BH2. Our results suggest that identifying systems with an an eccentricity greater than ∼0.5, or with black hole mass $M_{\rm BH}$ exceeding 10 $M_\odot$, would provide compelling evidence for their dynamical formation. With new detections from future Gaia data releases expected over the next few years, these results will help disentangle the formation channels of BH–star systems and the characteristics of the BH population in the MW.

Finally, our analysis also revealed the presence of some BH–giant systems[7] with $3\,M_\odot < M_{\rm BH} < 5\,M_\odot$, i.e., below the minimum BH mass allowed by the rapid supernova mechanism (Fryer et al. 2012). These peculiar systems form through accretion of matter by neutron stars from their binary companions, leading to the formation of BHs through accretion-induced collapse. None of these systems are

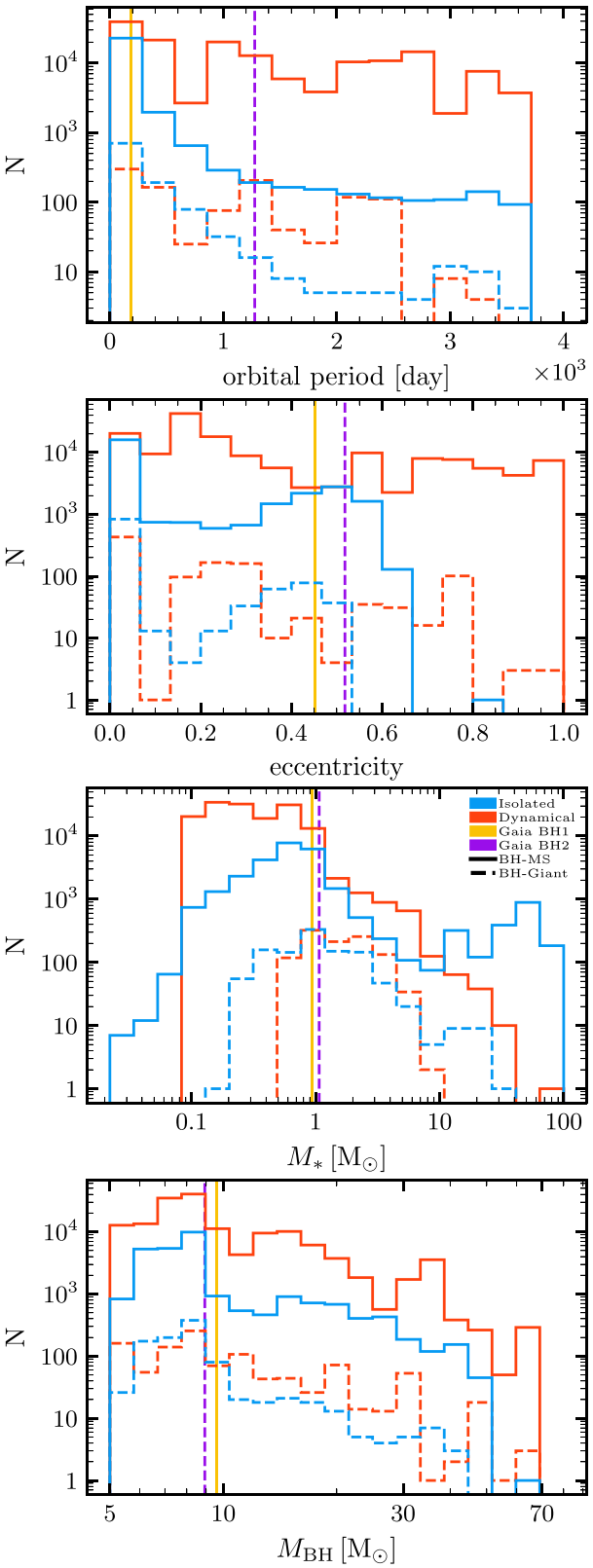

Figure 7. Distributions of orbital parameters of systems in the intrinsic population, including systems with age <100 Myr. From top to bottom: orbital period, orbital eccentricity e, star mass M_*, and BH mass $M_{\rm BH}$. SC binaries are shown by red lines, IB are shown by blue lines. Solid lines represent BH–MS binaries, while dashed lines show BH–giant binaries. The yellow and purple vertical lines represent the values of Gaia BH1 and Gaia BH2 respectively.

[7] For clarity, we have chosen not to include these systems in the plots presented in this paper.

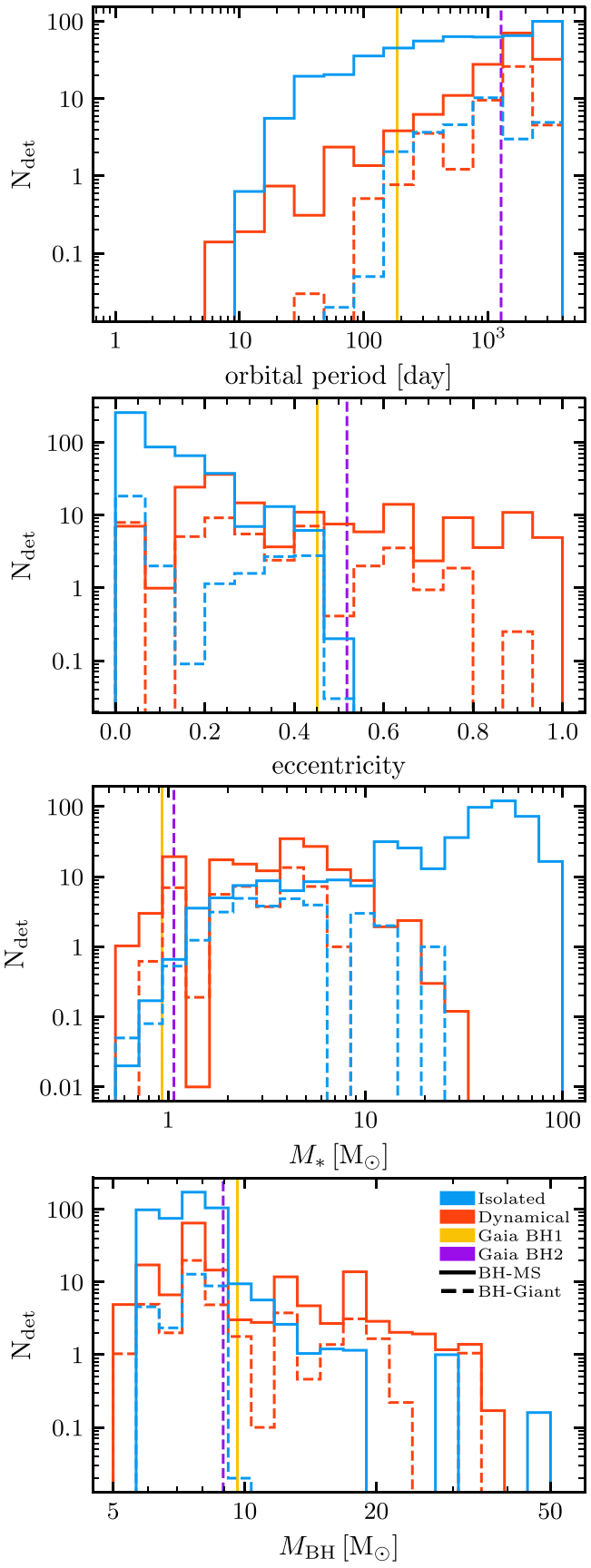

Figure 8. Same as Figure 7, but for systems detectable in future Gaia data releases.

detectable by Gaia according to our analysis, but we have not yet compared these systems (identified only in the IB channel) to their dynamical counterparts. Efforts to better characterize these systems are currently underway.

Acknowledgments

We thank Michela Mapelli, Sara Rastello, Giuliano Iorio, and all the members of the DEMOBLACK group for the useful discussions. U.N.D.C. thanks Daria Desiderà for the useful comments. This work was supported by NSF Grant AST-2009916 to The University of North Carolina at Chapel Hill and Carnegie Mellon University. The *N*-body simulations of young star clusters adopted here are an open-data product of the European Research Council (ERC) Consolidator grant DEMOBLACK, contract no. 770017 (PI: Michela Mapelli). C. R. acknowledges support from a Charles E. Kaufman Foundation New Investigator Research Grant, an Alfred P. Sloan Research Fellowship, and a David and Lucile Packard Foundation Fellowship. The Flatiron Institute is supported by the Simons Foundation.

ORCID iDs

Ugo Niccolò Di Carlo https://orcid.org/0000-0003-2654-5239
Poojan Agrawal https://orcid.org/0000-0002-1135-984X
Carl L. Rodriguez https://orcid.org/0000-0003-4175-8881
Katelyn Breivik https://orcid.org/0000-0001-5228-6598

References

Ballone, A., Mapelli, M., Di Carlo, U. N., et al. 2020, MNRAS, 496, 49
Ballone, A., Torniamenti, S., Mapelli, M., et al. 2021, MNRAS, 501, 2920
Bovy, J., Rix, H.-W., Green, G. M., Schlafly, E. F., & Finkbeiner, D. P. 2016, ApJ, 818, 130
Breivik, K., Chatterjee, S., & Larson, S. L. 2017, ApJL, 850, L13
Breivik, K., Coughlin, S., Zevin, M., et al. 2020, ApJ, 898, 71
Chakrabarti, S., Williams, T. G., Druard, C., et al. 2022, MNRAS, 520, 1815
Chawla, C., Chatterjee, S., Breivik, K., et al. 2022, ApJ, 931, 107
Corral-Santana, J. M., Casares, J., Muñoz-Darias, T., et al. 2016, A&A, 587, A61
Di Carlo, U. N., Giacobbo, N., Mapelli, M., et al. 2019, MNRAS, 487, 2947
Di Carlo, U. N., Mapelli, M., Bouffanais, Y., et al. 2020a, MNRAS, 497, 1043
Di Carlo, U. N., Mapelli, M., Giacobbo, N., et al. 2020b, MNRAS, 498, 495
Di Carlo, U. N., Mapelli, M., Pasquato, M., et al. 2021, MNRAS, 507, 5132
Drimmel, R., Cabrera-Lavers, A., & López-Corredoira, M. 2003, A&A, 409, 205
Drout, M. R., Massey, P., & Meynet, G. 2012, ApJ, 750, 97
El-Badry, K., Rix, H.-W., Cendes, Y., et al. 2023a, MNRAS, 521, 4323
El-Badry, K., Rix, H.-W., Quataert, E., et al. 2023b, MNRAS, 518, 1057
Fryer, C. L., Belczynski, K., Wiktorowicz, G., et al. 2012, ApJ, 749, 91
Gaia Collaboration, Vallenari, A., Brown, A. G. A., et al. 2022, A&A, 674, 22
Garmany, C., Conti, P., & Massey, P. 1982, ApJL, 263, L33
Giacobbo, N., & Mapelli, M. 2018, MNRAS, 480, 2011
Giacobbo, N., & Mapelli, M. 2019, MNRAS, 482, 2234
Giacobbo, N., & Mapelli, M. 2020, ApJ, 891, 141
Giacobbo, N., Mapelli, M., & Spera, M. 2018, MNRAS, 474, 2959
Giesers, B., Dreizler, S., Husser, T.-O., et al. 2018, MNRAS, 475, L15
Giesers, B., Kamann, S., Dreizler, S., et al. 2019, A&A, 632, A3
Goldberg, D., & Mazeh, T. 1994, A&A, 282, 801
Goodwin, S. P., & Whitworth, A. P. 2004, A&A, 413, 929
Green, G. M., Schlafly, E., Zucker, C., Speagle, J. S., & Finkbeiner, D. 2019, ApJ, 887, 93
Hafen, Z., Stern, J., Bullock, J., et al. 2022, MNRAS, 514, 5056
Holl, B., Fabricius, C., Portell, J., et al. 2023, A&A, 674, A25
Hopkins, P. F. 2015, MNRAS, 450, 53
Hopkins, P. F., Wetzel, A., Kereš, D., et al. 2018, MNRAS, 480, 800
Hurley, J. R., Pols, O. R., & Tout, C. A. 2000, MNRAS, 315, 543
Hurley, J. R., Tout, C. A., & Pols, O. R. 2002, MNRAS, 329, 897
Kroupa, P. 2001, MNRAS, 322, 231

Küpper, A. H. W., Maschberger, T., Kroupa, P., & Baumgardt, H. 2011, MNRAS, 417, 2300
Lada, C. J., & Lada, E. A. 2003, ARA&A, 41, 57
Licquia, T. C., & Newman, J. A. 2015, ApJ, 806, 96
Lindegren, L., Hernández, J., Bombrun, A., et al. 2018, A&A, 616, A2
Ma, X., Hopkins, P. F., Wetzel, A. R., et al. 2017, MNRAS, 467, 2430
Mapelli, M., Giacobbo, N., Ripamonti, E., & Spera, M. 2017, MNRAS, 472, 2422
Mapelli, M., Spera, M., Montanari, E., et al. 2020, ApJ, 888, 76
Marks, M., & Kroupa, P. 2012, A&A, 543, A8
Marshall, J. P., Cotton, D. V., Bott, K., et al. 2016, ApJ, 825, 124
Mazeh, T., Goldberg, D., Duquennoy, A., & Mayor, M. 1992, ApJ, 401, 265
McClintock, J. E., Shafee, R., Narayan, R., et al. 2006, ApJ, 652, 518
Moe, M., & Di Stefano, R. 2017, ApJS, 230, 15
Morton, T. D., 2015 isochrones: Stellar model grid package, Astrophysics Source Code Library, ascl:1503.010
Peters, P. C. 1964, PhRv, 136, 1224
Portegies Zwart, S. F., McMillan, S. L., & Gieles, M. 2010, ARA&A, 48, 431
Portegies Zwart, S. F., Verbunt, F., & Ergma, E. 1997, A&A, 321, 207
Rastello, S., Iorio, G., Mapelli, M., et al. 2023, MNRAS, 526, 740
Reed, B. C. 2003, AJ, 125, 2531
Remillard, R. A., & McClintock, J. E. 2006, ARA&A, 44, 49
Sana, H., de Mink, S. E., de Koter, A., et al. 2012, Sci, 337, 444
Tanikawa, A., Cary, S., Shikauchi, M., Wang, L., & Fujii, M. S. 2024, MNRAS, 527, 4031
Tanikawa, A., Hattori, K., Kawanaka, N., et al. 2023b, ApJ, 946, 79
Torniamenti, S., Ballone, A., Mapelli, M., et al. 2021, MNRAS, 507, 2253
Torniamenti, S., Rastello, S., Mapelli, M., et al. 2022, MNRAS, 517, 2953
Trani, A. A., Rastello, S., Di Carlo, U. N., et al. 2022, MNRAS, 511, 1362
Wang, L., Spurzem, R., Aarseth, S., et al. 2015, MNRAS, 450, 4070
Wang, L., Spurzem, R., Aarseth, S., et al. 2016, MNRAS, 458, 1450
Wetzel, A. R., Hopkins, P. F., Kim, J.-h., et al. 2016, ApJL, 827, L23